



# The CsI-based ring imaging detector for the ALICE experiment: technical description of a large prototype

for the ALICE collaboration

F. Piuz<sup>a,\*</sup>, Y. Andres<sup>a</sup>, A. Braem<sup>a</sup>, M. Davenport<sup>a</sup>, A. Di Mauro<sup>a</sup>, B. Goret<sup>a</sup>,  
A. Grimaldi<sup>b</sup>, P. Martinengo<sup>a</sup>, E. Monno<sup>b</sup>, E. Nappi<sup>a,b</sup>, G. Paic<sup>a,c</sup>, F. Posa<sup>b</sup>,  
J. Raynaud<sup>a</sup>, J.C. Santiard<sup>a</sup>, S. Stucchi<sup>a</sup>, G. Tomasicchio<sup>b</sup>, T.D. Williams<sup>a</sup>

<sup>a</sup>CERN, European Organization for Nuclear Research, Geneva, Switzerland

<sup>b</sup>INFN and Dipartimento Interateneo di Fisica dell'Università di Bari, Bari, Italy

<sup>c</sup>Ohio State University, Columbus, OH USA

---

## Abstract

We report on the design and construction of a CsI-RICH detector composed of four CsI photocathodes of  $64 \times 40 \text{ cm}^2$  each, and two  $\text{C}_6\text{F}_{14}$  radiator trays of  $133 \times 41 \text{ cm}^2$ . A detailed description of the novel elements is given and the performance of the detector is illustrated with some basic results obtained during the tests at the beam. © 1999 Elsevier Science B.V. All rights reserved.

---

## 1. Introduction

In a series of three papers, we report about the performance of the prototype of a Ring Imaging Cherenkov detector based on a cesium iodide (CsI) photoconverter, the CsI-RICH. The technical description of the large prototype is presented in this report, while the final test results and a study dedicated to Cherenkov angular resolution and simulation are described in Refs. [1,2], respectively. The CsI-RICH detector was proposed to form the High Momentum Particle Identification system (HMPID) of the ALICE experiment [3]. This system will be composed of seven modules, of  $1.3 \times 1.3$

$\text{m}^2$  each, aiming to complement the particle identification of the ALICE detector barrel in the 1.5–5 GeV/c momentum range. A detailed presentation of the HMPID system, including the associated R&D results can be found in Ref. [4].

## 2. Description of the prototype

### 2.1. The photodetector

The main components of the detector are shown in Fig. 1 as a cross-section and in Fig. 2 in isometric projection. In Fig. 2 the final HMPID module is represented, based on six pad panels and three radiator trays. The prototype was built according to the same design but reduced to four pad panels

---

\* Corresponding author.

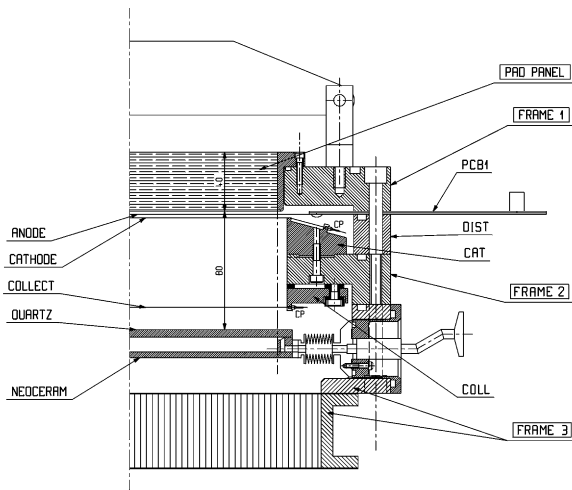


Fig. 1. Cross-section of the CsI-RICH prototype in a plane parallel to the anode wires.

a way that simple machining ensures:

- the parallelism and a controlled thickness of the two anode-to-cathode gaps of the MWPC,
- the parallelism between the radiator trays and the photodetector.

Peralumin is used as the material for the frame to guarantee optimum surface quality (porosity, polishing) and flatness during machining. The sealing between the frames is achieved by machining standard grooves for the Viton O-ring joints. In order to minimize the outgassing, care was taken to reduce the use of composite, organic material and gluing, in favour of metallic components. We shall describe the production of the pad cathode panel and frames, and the related assembly procedures.

### 2.1.1. The pad cathode panel

Given the particle density expected in the HMPID detector [3], a pad size of  $8 \times 8 \text{ mm}^2$  has been adopted providing the readout granularity adequate to achieve the Cherenkov ring pattern recognition [4]. The pad panel is assembled as a sandwich composite structure inserted in a metallic frame. This technology provides a stiff structure with a minimum of material and efficient gas sealing of the pad panels. The panel structure is schematically shown in Fig. 4. The composite structure consists of the pad-PCB and Kapton circuits, spaced by a 40 mm thick foam plate, from another circuit referred to as the ground-PCB. The Kapton foils are soldered on the pad-PCB in rows, leaving a free space of about 30 mm between them, for placing foam strips of that width. The grooves thus formed allow the Kapton foils to come out through apertures created in the ground-PCB. The pad-PCB is first glued to the frame on a granite table and the necessary ground connections made with conductive glue. Then, the elements are stacked and glued together under proper load, keeping the pad-PCB in contact with the granite table. A flatness of  $\pm 50 \mu\text{m}$  is achieved over an area of  $64 \times 40 \text{ cm}^2$ . The ground-PCB provides a well grounded electromagnetic shielding. The pins necessary for plugging the front-end (FE) electronics boards are implemented last. Besides acting as a pad-segmented MWPC cathode, the pad-PCB of the pad panel also acts as the substrate of the

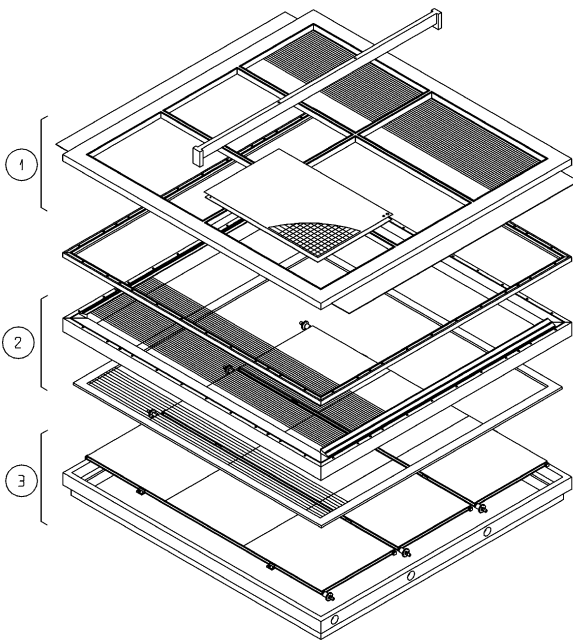


Fig. 2. Isometric view of a HMPID module. (1), (2), (3) are the elements described as Frame-1, Frame-2, Frame-3, respectively.

and two radiator trays, keeping the same dimensions in the other direction. Fig. 3 shows the prototype when installed at the test-beam line.

The detector is constructed by stacking a series of independent metallic frames designed in such

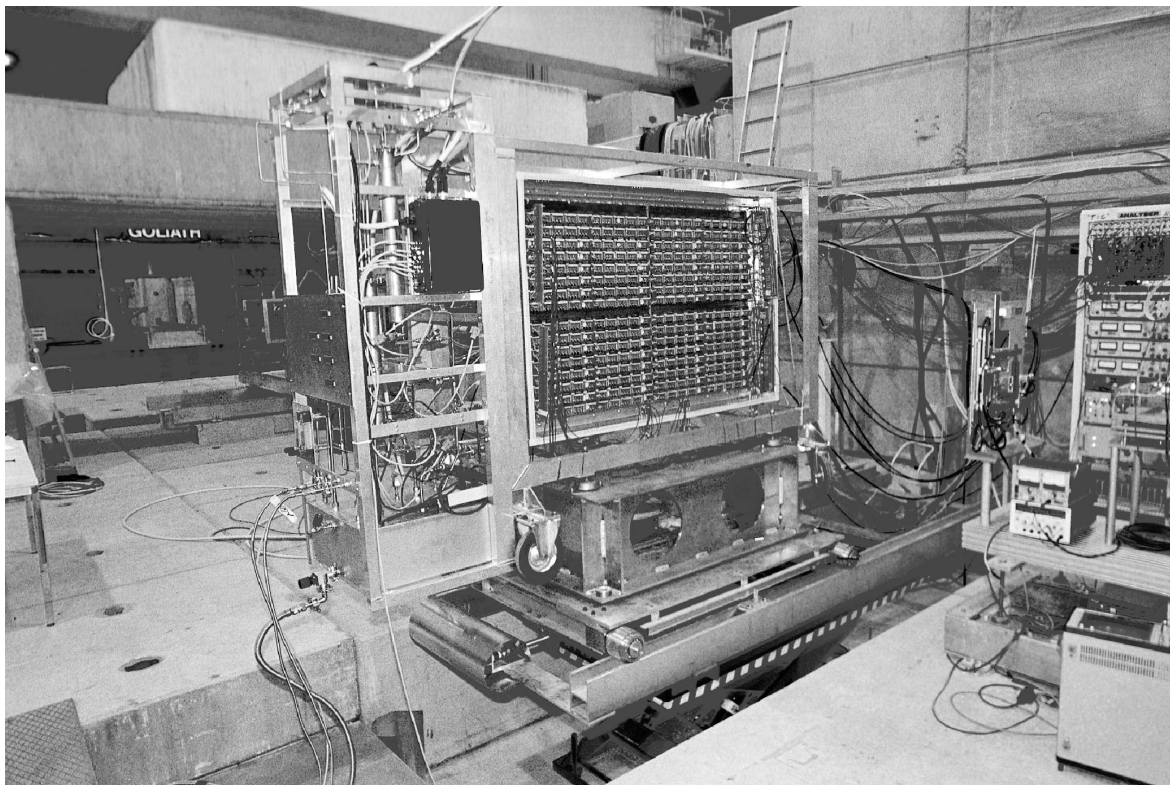


Fig. 3. View of the CsI-RICH prototype placed on a moving stage at the SPS-H4 test beam line. One sees the cathode pad panels instrumented with the FE electronics. On the left side, the system, used to control the  $C_6F_{14}$  circulation into the radiator trays, is attached to the detector hood.

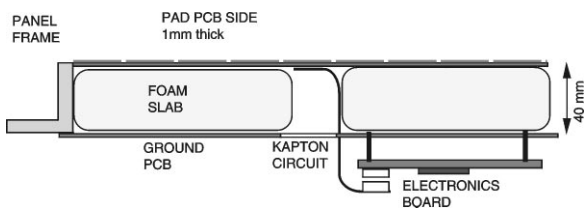


Fig. 4. Schematic cross-section of the pad panel. The foam is Rohacel-51-HF<sup>1</sup>. The glue in use is Araldite epoxy AW106-HV 953-4.

photocathode, meaning that all the pads are coated, under vacuum, with a CsI film, preserving the electrical connections to the FE electronics, ensuring optimum sealing with respect to the chamber gas.

<sup>1</sup> ROEHM GMBH Ruchstückstrasse, 8 PostfachCH8305 Bruttisellen, Switzerland.

After some development work, a dedicated PCB fabrication procedure was established such that large CsI layers of expected quantum efficiency performance could be produced with a good yield [4]. Two main problems were identified: (i) in order to avoid a destructive reactive contact between the CsI film and copper substrate, it was decided to cover the copper surfaces with a  $7\ \mu\text{m}$  nickel layer, known to be sufficiently dense, (ii) more care was devoted to surface preparation by using mechanical and chemical polishings. The nickel layer was in turn covered with a  $0.5\ \mu\text{m}$  layer of gold. Two alternative procedures are still under consideration, using two- or three-layer circuits, as shown in Fig. 5. In order to minimize the length of connections between the pads and FE channels and their dispersion, groups of 48 pad channels are made corresponding to a pattern of  $8 \times 6$  pads in the X and Y coordinates, respectively. The connection

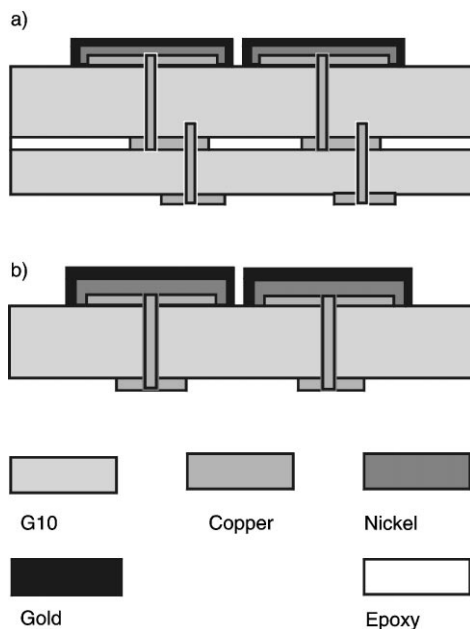


Fig. 5. Schematic cross-sections of the pad PCB: (a) version without through holes: the PCB is composed of two layers allowing for breaking the electrical connection between the pad and the external trace in two independent segments; (b) version with through holes. The polishings are applied to the copper clad before depositing the nickel layer. The total thickness is 0.8 mm.

is established by soldering flexible Kapton foils on the back of the pad-PCB, equipped at the other end with an SMD flat connector (ERNI-004863) with 50 contacts, which will be plugged into the FE board to ensure easy dismounting of the FE electronics.

### 2.1.2. Frames

*Frame-1.* As shown in Figs. 1 and 2, Frame-1 holds the elements forming half of the wire chamber, i.e. the pad cathodes and the anode wire plane. The described design allows the gap value and the parallelism of the two planes to be controlled within  $\pm 50 \mu\text{m}$ , allowing the pad cathode to be removed with a simple procedure without affecting the MWPC geometry. For this purpose, Frame-1 consists of a plate with four openings in which four pad cathode panels are easily mounted from the outside, tightened with screws and sealed with O-rings.

### The anode wire plane: installation and HV supply.

On the opposite side to the pad panel, the anode wires are stretched between two PCBs glued on opposite edges of the frame (PCB1 in Fig. 1). The wires<sup>2</sup> are 20  $\mu\text{m}$  in diameter, tungsten rhenium gold plated, 861/60, grade L, quality 4. The anodic wires are spaced by 4 mm. As the two PCBs are glued in grooves, further machining is necessary to adjust them to the same level as the frame and to ensure a flat surface for the O-ring to run over.

As the cathode pads are held at ground potential, the high voltage must be applied to the anode wires. The PCBs are designed such that they act as a high voltage feedthrough for every wire, by using a three-layer PCB configuration. Outside the chamber and at each end of the anodic wires, traces are pulled in groups of eight to a well-insulated flat connector. On one side of the chamber, a PCB is used to make the HV distribution. Each wire is fed through a 1 M $\Omega$  resistance implemented on small cards grouping eight resistors. All these cards can, in turn, be fed by traces linked to the HV supply. It has been checked that in the case of possible sustained discharges (loose wire), one or several wires could be disconnected from the HV source without affecting the operation of the remainder of the wire plane, allowing for easy localization of the defective wire. The connectors available on the opposite PCB may be used for implementing electronics for reading out fast wire signals or checking the anode wire tension by using the CAEN instrument SY502.

Given the length of the anode wires of 120 cm, a support line structure is needed to ensure the stability of the wires against the electrostatic force. For assembly reasons and since the second MWPC cathode consists of wires, this element can only be implemented between the pad cathode and the anodic wire plane. To give the correct spacing, the anodic wires are positioned using a comb, stretched by a weight of 40 g and held to the PCB by tin soldering. The wires are located in thin triangle-shaped grooves, 0.2 mm deep, machined at the surface of the Macor support line. For optimum safety (against vibrations, etc.), a very small amount

<sup>2</sup> Luma Metall Lumalampan AB, PO BOX 701, S-391 27 Kalmar, Sweden.

of glue (AV144-2/HV 997) was added, thus fixing the wires in these grooves.

Once the anode plane has been soldered, the distance between this plane and the upper side of Frame-1 is measured at several points all around the frame. The thickness of each pad panel is also measured at several points between the pad surface and the inner side of its frame. After averaging and adjustments, the difference between these two measurements must be made equal to the nominal distance anode-to-pads, i.e. 2 mm. This is possible by machining, if necessary, the inner side of the pad-frame in the final adjustment.

*Frame-2.* The frame-2 holds two wire planes and its thickness contributes to the depth of the proximity gap of the RICH (see Figs. 1 and 2). One of the wired planes is the second cathode of the MXPC photodetector that is kept at ground potential. It is made of 100  $\mu\text{m}$  diameter gold plated Cu/Be wire, spaced by 2 mm. This spacing ensures 95% transparency to the incident Cherenkov photons and acts as an electric screen between the proximity and MWPC gaps. In order to avoid having a new PCB for holding these wires, crimping pins were used to support the stretching tension, fixed at 200 g/wire. Two independent machined bars are used to position and plug in the metallic crimping pins, allowing thus simpler drilling than in the case of a monolithic frame. The reason these bars have an oblique side (see Fig. 2) is to create a shape surrounding the edge of the PCB where the 20  $\mu\text{m}$  wires at HV are soldered, such that the distances are much larger than the 2 mm gap. In this zone, the electrical field is kept at a low level, thus avoiding any breakdown from the anodes to surrounding grounds. The PCB is also long enough to avoid any leakage current along the circuit surface (see next section). Once the cathode is wired, the distance between the wire plane and the upper side of Frame-2 is measured all around the frame. Then, the gap between the wired cathode and the anode planes can be adjusted to its nominal value, 2 mm, by machining the distance frame, interleaved between Frame-1 and Frame-2 to the necessary thickness.

The second wire plane is the collection electrode which creates a small electric field in the proximity gap in order to drain primary ionization, deposited by the particles, instead of drifting into the MWPC

gap and inducing too large signals. This electrode is fixed to the frame-2 by means of an independent frame. It is made of the same 100  $\mu\text{m}$  diameter gold plated Cu/Be wire spaced by 5 mm also using crimping pins. It is held at a voltage of about 300 V. The gap between the collection electrode and the radiator tray should be kept to a minimum since primary ions created in that interval are repelled against the insulated radiator window and might create deposits.

*Frame-3.* A light composite panel is fixed on Frame-3 to close the detector (see Figs. 1 and 2) made by sandwiching 50 mm of an aramide-fibre epoxy honeycomb material between two 0.5 mm thin layers of aluminium (Fig. 1). The radiator trays are held by guiding parts attached to the panel.

### 2.1.3. Main results about the operation of the detector

The 1  $\text{m}^2$  area of the prototype delivers a dark current of 1–2 nA; during local beam irradiation, up to  $2 \times 10^4 \text{ cm}^{-2} \text{ s}^{-1}$ , a stable operation is achieved and the current is about 20 nA, with the collection electrode voltage  $V_{\text{coll}}$  set to 250 V and the anode wires voltage set to 2050 V.  $V_{\text{coll}}$  has been optimized by measuring the current in the chamber irradiated by particles at a rate of  $9 \times 10^3$  per burst. It has been observed that the chamber current decreases and stabilizes when  $V_{\text{coll}}$  is larger than 150 V, fully restricting the signals of charged particles to the primary ionization deposited in the thin MWPC gap.

In Fig. 6, we show the variation of the single-electron mean PH,  $A_0$ , as a function of the chamber voltage for the different gas mixtures that were tested. The working voltage range starts at an  $A_0$  value of 10–15 ADC channels. Remembering that the FE electronics threshold,  $A_{\text{th}}$ , is of 3–4 ADC channels, single-electron detection efficiencies are obtained as  $\exp(-A_{\text{th}}/A_0)$ .

### 2.2. The radiator array

The high  $\text{C}_6\text{F}_{14}$  and  $\text{SiO}_2$  densities, 1.68 and 2.1  $\text{g}/\text{cm}^3$ , respectively, and the need to minimize the total amount of material traversed by the incoming particles, required a careful investigation to optimize the radiator vessel mechanical structure. In

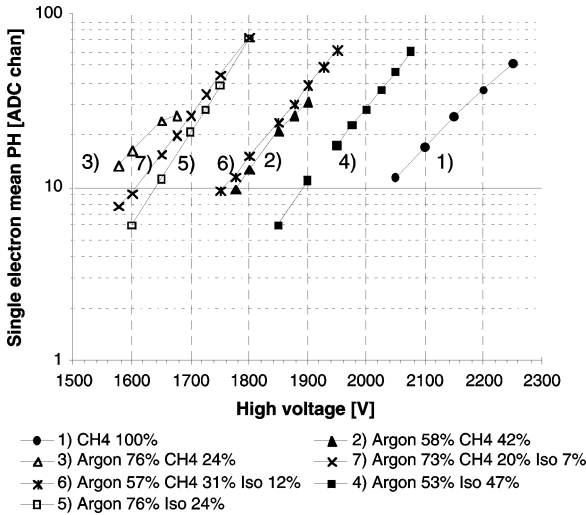


Fig. 6. Variation of the mean single-electron pulse height,  $A_0$ , as a function of the chamber anode voltage for different gas mixtures. Measurements were obtained with a 10 mm  $C_6F_{14}$  radiator at the H4/SPS beam line, 350 GeV/c pions. One ADC channel corresponds to 0.17 fC.

addition, since the HMPID performance depends strongly on transparency in the UV spectral range 160–220 nm and long-term stability of the  $C_6F_{14}$  radiator, the emphasis was put on the choice of materials.

### 2.2.1. Radiator description

The liquid radiator container consists of a tray made of a glass-ceramic material called Neoceram,<sup>3</sup> closed by a UV-grade fused silica plate, as shown in Fig. 7. The thermal coefficient of Neoceram ( $0.5 \times 10^{-6} \text{C}^{-1}$ ) ensures that no mechanical stress is induced on the vessel by temperature gradients. The limited size of commercially available fused silica plates and the need to keep the hydrostatic load within reasonable levels determined the thickness and size of the radiator vessel elements: in the current geometry, the quartz window is 5 mm thick, whilst the Neoceram base plate is 4 mm thick. The vessel elements are glued together with Araldite AW106. The liquid radiator inlet and outlet are obtained by gluing two stainless-steel pipes on the opposite sides of the Neoceram tray, the outlet

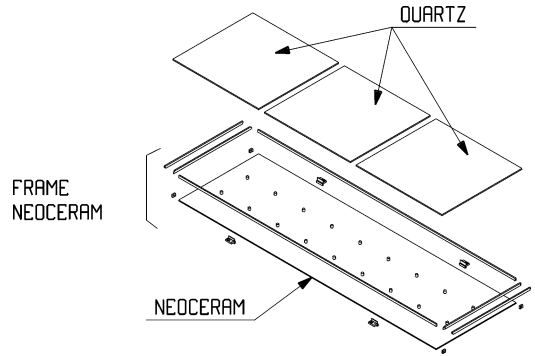


Fig. 7. Isometric view of the elements composing a radiator tray. Four carbon fibre feet are used to locate the tray in the detector back plane (Frame-3).

Table 1  
Material budget

	Material thickness (mm)	$X/X_0$
Honeycomb back panel	50	0.02
Neoceram plate	4	0.03
Quartz window	5	0.05
$C_6F_{14}$	10	0.05
PC panel + FEE	1	0.02

always being at the highest location. To withstand the hydrostatic pressure, 24 cylindrical spacers are glued to the bottom plate on one side and to the quartz window on the other side. The spacers consist of fused silica rods with a diameter of 10 mm; they are placed in two rows of 12 equidistant elements.

The prototype has two independent radiator trays, of size  $133 \times 41 \text{ cm}^2$ , supported by a stiff composite panel (Frame-3). The radiator vessel and the fluid dominate the bulk of the detector material, estimated to be 17%  $X_0$  (Table 1).

### 2.2.2. Assembly of the radiator tray

Before gluing, all elements must be carefully cleaned to remove any trace of pollutants on the surfaces. The radiator is assembled by gluing the Neoceram pieces to the quartz windows in a dust-free room kept at 35°C with a relative humidity of less than 50%. An optical table is used for assembly

<sup>3</sup> Nippon Electric Glass Co., Ltd., Japan.

to ensure the right flatness over the whole surface of the radiator. All gluing steps are performed by using a home-made tool that distributes the Araldite AW-106 at a constant rate to ensure a glue thickness of 0.15 mm everywhere. The quartz window is obtained by gluing the three constituent plates using a tool specially built to guarantee a final flatness of the resulting plate better than 0.05 mm.

### 2.2.3. Test results

A full-scale prototype of the liquid radiator vessel was made using only Neoceram elements, with 16 equidistant spacers, and tested in several hydrostatic loading conditions. Strain, stress and deflection states of the two base plates measured in the test were compared with a Finite Element Analysis (FEA) by means of the IDEAS<sup>4</sup> software package. Tests were executed by overloading the radiator vessel prototype, filled with C<sub>6</sub>F<sub>14</sub>, with an extra 200 mm of liquid column corresponding to a maximum pressure of 103 mbar for the vertical position and 131 mbar for the most critical orientation. In addition, stress and deformation data were recorded by overloading the radiator vessel with 100 mm of liquid column. The main results found in Tables 2 and 3 have finally led to a spacer configuration of 24 elements guaranteeing a safety coefficient of 7 under maximum constraints.

Once we have assessed the behaviour of the tray under normal operation conditions, two radiator trays were built and installed in the prototype. The following tests were performed at the end of the radiator vessel assembly phase in order to ensure that each part works properly:

- (i) tightness test and measurement of the He diffusion rate through the vessel quartz plates, performed by using a He sniffer; satisfactory results were obtained, as no appreciable leak was detected above  $3 \times 10^{-7}$  atm cm<sup>3</sup> s<sup>-1</sup>;
- (ii) C<sub>6</sub>F<sub>14</sub> circulation test and pressurization test.

Table 2

Comparison between the test measurements and the FEA evaluation

	Measurement	Finite-element method
Maximum stress $\sigma$	12.5 N/mm <sup>2</sup>	12.7 N/mm <sup>2</sup>
Plate deflection	0.081 mm	0.079 mm

Table 3

Maximum principal stress (N/mm<sup>2</sup>) versus C<sub>6</sub>F<sub>14</sub> hydrostatic pressure in the radiator tray with 24(18) spacers ( $h = 0$  corresponds to the full radiator, while  $h = 100$  corresponds to an additional liquid column 100 mm high, that takes into account the anticipated overpressures due to the liquid circulation system). The bending strengths for the quartz and Neoceram plates are 67 and 100 N/mm<sup>2</sup>, respectively

Radiator tray element	$h = 0$	$h = 50$	$h = 100$
Quartz plate	8.31(11.16)	9.00(12.26)	9.68(13.36)
Neoceram plate	11.6(16.93)	12.72(18.63)	13.84(20.33)
Quartz spacers	7.36(10.91)	8.12(12.06)	8.88(13.20)
Neoceram frame	4.10(4.33)	4.47(4.73)	4.84(5.13)

## 2.3. The C<sub>6</sub>F<sub>14</sub> circulation system

A liquid recirculation system was designed and built at CERN for the beam tests of the prototype at the CERN/SPS during 1997 and 1998. The system was required to purify, fill, recirculate and empty two liquid C<sub>6</sub>F<sub>14</sub> radiator trays independently, remotely and safely. The liquid distribution to and from the radiators was based on a gravity flow principle, similar to that implemented by the CRID group at SLD [6]. A schematic description is shown in Fig. 8.

### 2.3.1. Liquid, construction materials and physical properties

The liquid chosen for the HMPID system was PF-5060DL (from 3M<sup>5</sup> company), with characteristics shown in Table 4. Note the high density, volatility and the high solubility of air and water. These characteristics influence the circuit design. The high density causes considerable hydrostatic

<sup>4</sup>SDRC (Structural Dynamics Research Corporation), 2000 Eastman Drive, Milford, OH 45150-2789, USA.

<sup>5</sup>3M Performance Chemicals and Fluids Division, St Paul, MN 51144-1000, USA.

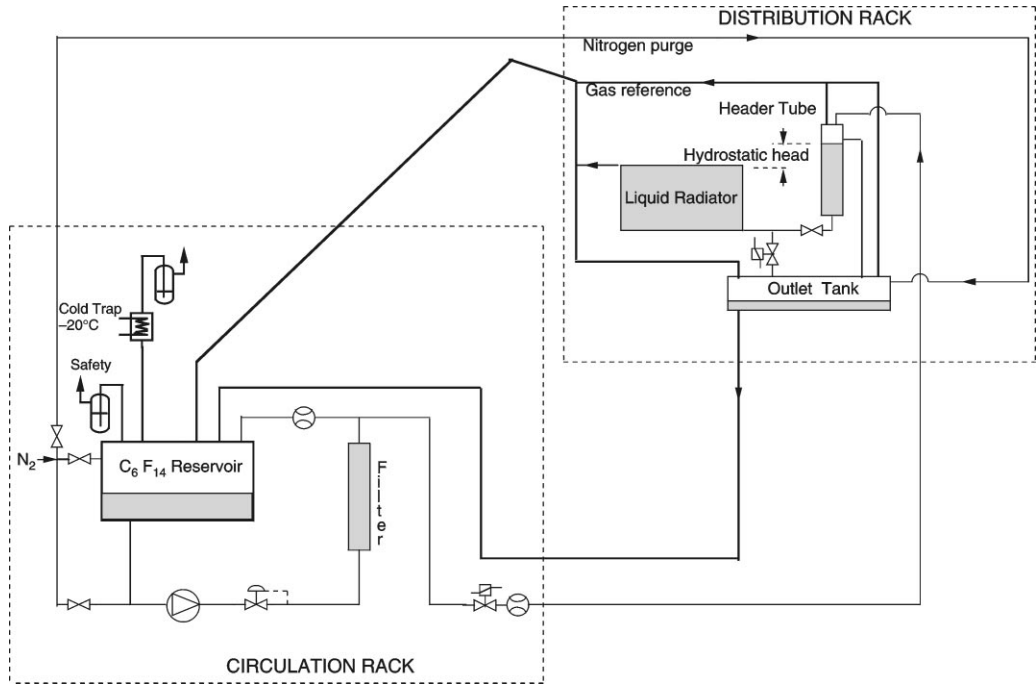


Fig. 8. Schematic of the C<sub>6</sub>F<sub>14</sub> circulation system. As seen in Fig. 3, the distribution rack is attached directly onto the detector.

Table 4  
Physical properties of PF-5060DL

ODP (ozone depletion potential)	0
Average molecular weight	338
Boiling point °C	56
Liquid density (g/ml @ 25°C)	1.68
Liquid viscosity (cSt @ 25°C)	0.40
Vapour pressure (mbar @ 25°C)	309
Solubility of H <sub>2</sub> O (ppm by weight @ 25°C)	10
Solubility of air [ml gas/100 ml liquid (FC-72)]	48
Solubility of oxygen [ml gas/100 ml liquid (FC-72)]	65
Thermal expansion coefficient @ 25°C (ml/ml °C × 10 <sup>3</sup> )	1.6
Refractive index (ND) @ 25°C (FC72)	1.251

loading on fragile optical windows; the volatility implies high evaporation losses, which must be recovered; the high solubility of air and water vapour results in over 100 000 vpm oxygen and about 10 000 vpm water vapour in the raw material. Since both of these gases are strongly absorbent in the UV they must be reduced to trace levels, to ensure

high optical transparency in our application (160–220 nm wavelength range).

### 2.3.2. Liquid recirculation, gravity flow

The liquid from the reservoir is pumped via cleaning filters towards each radiator. The liquid first enters a header tube located above the radiator. The top of the tube is connected to the gas reference system; the bottom is connected via a valve to the low point of the radiator. The tube acts as a hydrostatic gravity feed for the radiator. It contains a large-diameter overflow pipe to limit the hydrostatic head (height difference between the overflow and the outlet at the top of the radiator). This head is set to produce the required flow through the filled radiator, taking into account the impedance of the filling line and the radiator. Liquid from the radiator outlet falls unimpeded into a large-diameter outlet tube, connected upward towards the gas reference network and downwards toward a large-volume liquid outlet tank. The outlet tube was constructed to eliminate any syphons. The circulation cycle starts with the

progressive filling of the header tube, which in turn generates flow to the radiator. The level in the tube reaches overflow and then remains constant. The radiator filling continues until the radiator overflows into the outlet line and down to the outlet tank. At this point the gravity feed and the flow through the radiator become constant. From the bottom of the outlet tank the liquid falls into a large diameter return line and back to the system reservoir. The outlet tank must always be above the level of the system reservoir to ensure return flow by gravity. The top of the outlet tank is connected to the gas reference network by lines without syphons. When the flow to the radiators is stopped, the hydrostatic head drains via the radiator. The radiator then remains full until circulation is restarted. The reference system is purged by a flow of 20 l/h pure N<sub>2</sub> and exhausted via a cold trap and an oil bubbler.

### 2.3.3. Operational experience: cleaning and liquid transparency

Tests were carried out during three test beam periods, where the C<sub>6</sub>F<sub>14</sub> circulation system was supplying two radiator trays, mounted in the CsI-RICH prototype. The circulation rack, the associated control system and the refrigeration system were located outside the beam area, connected via standard stainless steel pipes to the distribution rack mounted onto the prototype (Fig. 8). The system was filled progressively with 35 l of C<sub>6</sub>F<sub>14</sub> and cleaned up in a closed-circuit circulation by passing through a molecular sieve cartridge (13X-1001 UETIKON<sup>6</sup>) and a mechanical filter (Ultrafilter<sup>7</sup> 1 μm). Then, the liquid flow was shared between the cleaning part and the detector system circulated at a flow of 6 l/h per radiator tray. After a period of about two weeks, the UV-transparency of the liquid was at the level of the expected performance, as seen in Fig. 9, and maintained at such a level during the whole test period. The loss of liquid coming from the condensation of C<sub>6</sub>F<sub>14</sub> vapour

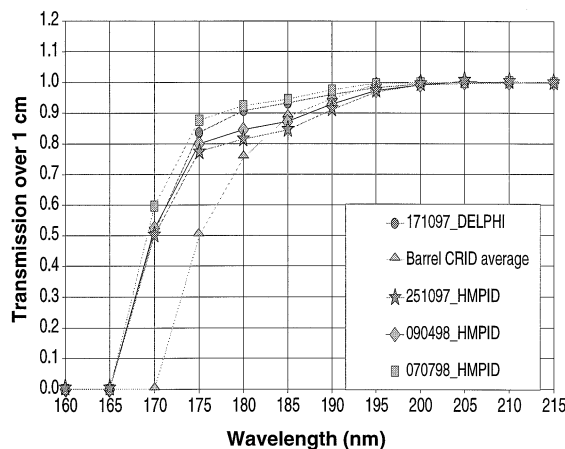


Fig. 9. C<sub>6</sub>F<sub>14</sub> UV-transparency curves comparing typical results obtained in other large systems with three measurements from the HMPID prototype, showing an improvement in the quality with time.

into the gas reference line was kept at about 1 l/week, having the cold trap system kept at –20°C. The system ran stably and safely during the three data taking runs. A detailed description of the elements and tests of the radiator and circulation systems is found in Ref. [4].

## 3. Production of large CsI photocathodes

The basic properties of the CsI film and the main procedures to achieve films of high QE performance are discussed in Refs. [4,5]. Here will be presented the CsI evaporation facility used to process all the PCs studied so far; it will be used as well for the final production of the HMPID PCs. The station is being extended with another vessel in which the freshly evaporated PC can be translated under vacuum and scanned for local evaluation of its QE.

### 3.1. CsI evaporation facility

The CsI evaporation facility is shown schematically in Fig. 10. The main body is a cylindrical vessel, made of stainless steel, of 0.8 m diameter, 1 m long, lying horizontally on a support and closed by rotatable doors to allow easy access from

<sup>6</sup>CU Chemie Uetikon GmbH, Raiffeisenstrasse 4, D-77933 Lahr, Germany.

<sup>7</sup>ULTRAFILTER AG, Thurgauerstrasse 74, CH-8050 Zurich, Switzerland.

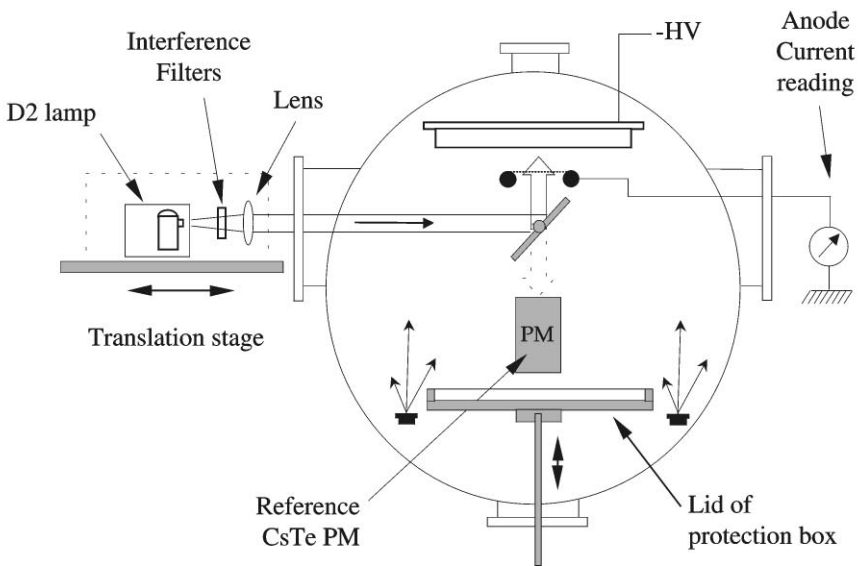
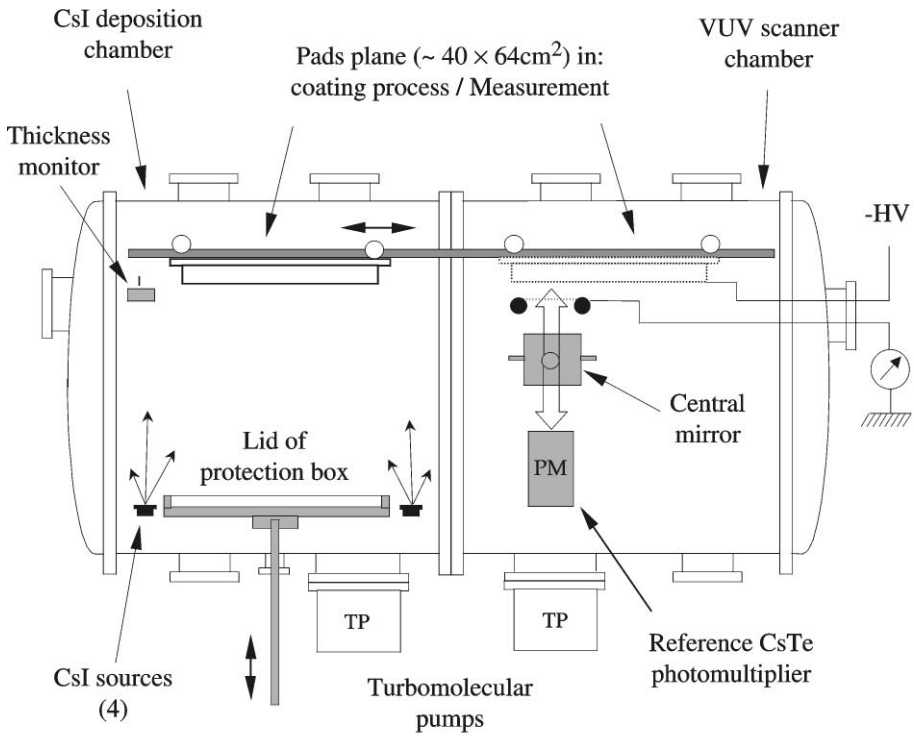


Fig. 10. Schematic side- and cross-views of the CsI evaporation system. (top) The evaporation and the QE measurement parts are on the left and on the right side, respectively. (bottom) Principle of the QE evaluation based on the measurement of the photocurrent produced by local irradiation of the CsI PC by a monochromatic UV beam, the intensity of which is obtained from a calibrated PM.

both ends. Side flanges are used to install auxiliary equipments such as pumps, pressure probes, electrical and motion feedthroughs, etc.

The primary and secondary vacuum are obtained from a 120 m<sup>3</sup>/h rotary pump and two turbo pumps (total evacuation speed of 2500 l/s), respectively, separated by a catalyser trap. Resistive heating bands are wound around the cylindrical vessel allowing the system to be heated up to about 100°C, for outgassing and temperature conditioning. A Quadrupole Mass Spectrometer Balzers QMS200 is now available to analyse partial pressures of residual gases. The residual pressure in the evaporation vessel after outgassing is  $2 \times 10^{-7}$  Torr, deteriorated to  $5 \times 10^{-7}$  Torr when a pad panel array is installed.

### 3.2. Manipulation of the pad panel

The side of the pad panel where the FE electronics connectors are implemented (ground-PCB in Fig. 5) is first enclosed in a box made of a metallic lid tightly fixed to the back of the pad panel. When installed inside the evaporator, a primary vacuum is independently made in this box as the full vessel is evacuated. In this way, we avoid an excessive outgassing expected from the FE-instrumented side and balance the pressure on both sides of the pad panel. Then, although only the clean pad face is exposed to vacuum, a long outgassing time is necessary to reach a total residual pressure of  $5 \times 10^{-7}$  Torr indicating that moisture is still present at the surface of the pad PCB. A second metallic lid is installed at the bottom of the evaporator, fixed on a motorized system, enabling it to be moved vertically inside the evaporator. This lid is designed in such a way that it constitutes, when put in contact with the pad panel, a tight box to protect the CsI film. After the CsI film has been deposited and the vessel filled with argon at atmospheric pressure, the lid is lifted and kept firmly pressed against the pad panel frame in order to compress the O-ring and ensure a good tightness even in the absence of screws. Then, the so-constituted box is flushed with argon at atmospheric pressure and the evaporator vented at the same time. After opening the evaporator,

the necessary screws are inserted to ensure the lid is tightened on the pad panel, the pressure exerted by the lifting device is released and the CsI pad panel is removed from the evaporator under inert gas protection, without being in contact with air.

### 3.3. CsI evaporation system

Given the diameter of the evaporator, the distance available from the boats to the substrate is about 50 cm. In order to ensure a uniform thickness of the CsI film over the large area of PCs, four evaporation boats are used. Their locations with respect to the PC are optimized such as to ensure a variation of the film thickness of no more than 10% over an area of  $65 \times 50$  cm<sup>2</sup>. The thickness of the CsI layers is typically in the 400–500 nm range. The boats are made of molybdenum and are heated independently by “direct current” Joule effect. The CsI loads are calculated such as to obtain the desired film thickness after complete evaporation of the four boats content. The CsI loads are pre-molten in the boats under vacuum in order to have a good thermal contact between the CsI and the boat and to avoid local overheating. The four boats are evaporated simultaneously under the control of a quartz Edwards FTM5, monitoring the evaporation rate and the thickness. During the first few seconds, a shutter masks the sources in order to prevent the deposition of possibly polluted material; then it is removed. A slight drop in pressure, of about 25% of the initial pressure, is usually observed at the beginning of the evaporation, probably as a consequence of the reduced outgassing of the vessel and of the pad panel, caused by the freshly deposited CsI layer.

### 3.4. Conditioning

After installation of the pad panel and the boats in the evaporator, the sequence of operations is as follows:

- pump and outgas for 2–3 days at 60°C until a residual pressure  $\leq 2 \times 10^{-6}$  Torr is reached;
- evaporate CsI on substrate maintained at 60°C, at a rate of about 5 nm/s;

- heat condition at 60°C under vacuum for 8–12 h, at a pressure  $\leq 2 \times 10^{-6}$  Torr;
- stop heating for cooling down to 40°C;
- venting the protection box and the evaporator with argon;
- lift the lid to form the protection box;
- open the evaporator and transfer the pad panel to storage under argon flow.

The transfer of the CsI pad panel to the detector is performed without exposure to air by using a dedicated 'glove box' fixed temporarily at the back of the detector and kept under inert gas circulation. The procedure is described in Ref. [4].

#### 4. Quality control of photocathodes: the VUV scanning set-up

Anticipating the production of a large number of CsI-PCs for the HMPID system, a simple and fast method has been elaborated for evaluating the PC performance just after processing. As schematized in Fig. 10, it is based on the direct measurement of the photocurrent emitted under a local illumination of the CsI PC by a monochromatic and collimated VUV light beam. A cylindrical vessel of the same size as the evaporator is appended to it to create a volume large enough to scan the PC. The set-up is composed of the following elements:

- A motorized linear motion, parallel to the cylinder axis ( $x$ -coordinate), which performs first the transfer of the pad panel from the evaporation to the measurement vessel and then moves the panel by steps for the scan.
- Perpendicular to the evaporator axis ( $y$ -coordinate), a mechanical structure supports another stage providing the motion of the measurement arm in the  $y$  direction. An expandable and tight connection is made between the stage and the measurement vessel by a bellows of 110 mm diameter, allowing a scan over 50 cm in the  $y$  direction.
- The VUV source, a D<sub>2</sub> lamp, its housing and the necessary CaF<sub>2</sub> optics, delivering the VUV collimated beam, are located on the  $y$ -moving stage. The UV beam is propagated through a tube up to a mirror fixed at the other extreme of the

measuring arm, reflecting the beam up or down, by a remotely controlled action. At the same end of the arm, a wire electrode is fixed, collecting the photoelectrons from the PC. This structure keeps the length of the UV beam and electrical connections fixed while the stage is moved for scanning purposes. Rotating the mirror by 90° directs the beam to a reference phototube, allowing the intensity of the incident photon flux to be calibrated. The phototube is a Hamamatsu R1460, 1 inch diameter, MgF<sub>2</sub> window. The CsTe photocathode response was calibrated against a NIST photodiode in the 150–220 nm range [7].

A dedicated slow-control monitoring task has been developed aiming to control the parameters during the CsI film processing phase (pressure, temperature, rate, etc.) and to perform automatic QE measurements by scanning large-area PCs.

#### 5. Conclusions

The design and construction of a large prototype of a CsI-RICH detector has been described. An emphasis was given to the description of elements specific to this novel detector, such as the production of large-area CsI photocathodes, the photodetector, the liquid radiator array and its associated C<sub>6</sub>F<sub>14</sub> circulation system. Results obtained during an extensive test at the beam illustrate the detector capability of being safely and steadily operated in the experimental conditions of the ALICE experiment. Following the approval of the CERN/LHC Committee, the next step will be the construction of seven modules, of  $\sim 2$  m<sup>2</sup> each, to be completed for the start of the ALICE experiment.

#### Acknowledgements

During the development and construction phase of the large prototype, the HMPID group was helped by the following technical teams: Mr. A. Gandi and the CERN Printed Circuit Workshop, Mr. C. Millerin and the EP/CERN Electronics

Workshop, the CERN/TA2, the DELPHI support groups and the Bari Technical Team. They are all gratefully acknowledged for their essential contributions.

## References

- [1] F. Piuz et al., Nucl. Instr. and Meth. A 433 (1999) 178.
- [2] A. Di Mauro et al., Nucl. Instr. and Meth. A 433 (1999) 190.
- [3] ALICE Collaboration, Technical Proposal, CERN/LHCC 95-71.
- [4] ALICE Collaboration, Technical Design Report of the High Momentum Particle Identifier Detector, CERN/LHCC 98-19.
- [5] A. Breskin et al., Nucl. Instr. and Meth. A 371 (1996) 116, and references therein.
- [6] K. Abe et al., IEEE trans. Nucl. Sci. 40 (1993) 4; SLAC-PUB-5888, 1992.
- [7] A. Breskin et al., Nucl. Instr. and Meth. A 343 (1994) 159.